Microgravity Science and Technology (2022) 34:92
https://doi.org/10.1007/s12217-022-10012-1

RESEARCH

Thermocapillary-enhanced Melting of Different Phase-change Materials in Microgravity

Nathaly García-Acosta[1] · Pablo Salgado Sánchez[1] · Jaime Jiménez[1] · Úrsula Martínez[1] · Jose Miguel Ezquerro[1]

Received: 7 June 2022 / Accepted: 26 August 2022 / Published online: 9 September 2022

Abstract

A numerical analysis of the thermocapillary-driven melting of phase change materials (PCMs) in weightlessness is presented. The phase change is explored for different PCMs with moderate melting temperatures, due to their potential for thermal control in space applications. We consider three different alkanes — n-octadecane, n-nonadecane, and n-eicosane — and gallium. Results are discussed in terms of the dimensionless Stefan (Ste) and Marangoni (Ma) numbers, which quantify the importance of the latent heat and the thermocapillary effect during the phase change process, respectively, and the container aspect ratio Γ. For alkanes, similar results are obtained with melting rate enhancements that depend on Γ. In short (deep) containers, the thermocapillary effect accelerates melting — with respect to the conduction-driven case — by a factor of as much as 4 depending on Ma, while in large (shallow) containers, this enhancement factor can take values up to 20. The best performance is featured by n-eicosane, followed closely by n-octadecane. For gallium, results differ substantially due to its high thermal diffusivity, leading to a significant reduction of the enhancement up to a value of approximately 1.2 at large Ma and Γ.

Keywords Phase change materials · Thermocapillary effect · Microgravity

Introduction

Nowadays, almost every equipment of daily use requires temperature control or can benefit from it (Chaiyat and Kiatsiriroat 2014; Lee and Medina 2016; Biwole et al. 2013; Ho et al. 2013). The incorporation of a phase change material (PCM) with large heat of fusion and appropriate melting temperature T_M increases thermal inertia and helps maintain the equipment temperature near T_M. When the system heats up, the PCM melts and absorbs energy in the form of latent heat. This energy is then released during solidification when it cools down. Thermal control is of special interest in the space sector, where PCM devices have been utilized in many important missions like the Venera 8-10 probes, the Lunar Rover Vehicle of Apollo 15, and Skylab SL-1 (Lane 1983; Creel 2007). Note that the particular thermal environment of orbiting spacecraft is often characterized by extreme variations of the solar heat flux, driving large temperature changes of periodic nature (Kim et al. 2013).

Different natural and synthetic PCMs with a wide spectrum of T_M are used to accommodate the variety of applications. Organic materials, like fatty acids and alkanes, are attractive due to their chemical stability and moderate T_M. Their effectiveness for thermal control, however, is generally compromised by low thermal conductivity and the associated slow diffusion of heat, leading to long melting and solidification cycles. To palliate this, a number of strategies have been proposed (Salgado Sanchez et al. 2020b). One straightforward idea is to improve diffusive transport by introducing conductive materials in the PCM device (Ettouney et al. 2004; Agyenim et al. 2009; Fernandes et al. 2012; Atal et al. 2016; Cabeza et al. 2002), or by increasing its thermal diffusivity with the addition of dispersed (conductive) nanoparticles; these are known as nano-enhanced PCMs (NePCMs) (Hosseinizadeh et al. 2012; Dhaidan et al. 2013; Mishra et al. 2022). An alternative way relies on geometrical PCM designs that promote natural convection in the liquid phase (Dhaidan and Khodadadi 2015). The associated convective transport is generally more effective and can substantially increase (reduce) the phase change rate (time).

✉ Pablo Salgado Sánchez
pablo.salgado@upm.es

[1] E-USOC, Center for Computational Simulation, Escuela Técnica Superior de Ingeniería Aeronáutica y del Espacio, Universidad Politécnica de Madrid, Plaza Cardenal Cisneros 3, 28040 Madrid, Spain

For space applications, however, none of the aforementioned strategies, except that of NePCMs, is convenient since they either increase notably the mass of the PCM device or rely on buoyant flows. In this context, the thermocapillary effect — whereas a nonuniform temperature induces surface tension gradients that drive convective flow — has been proposed as a simple alternative to enhance heat transport and overall PCM performance in microgravity. The relevance of thermocapillary flows has long been recognized in many technological processes like welding (Samanta 1987; Shuja et al. 2011), combustion (Sirignano and Glassman 1970; Higuera 2002), and other phenomena like crystal growth (Schwabe and Scharmann 1979; Preisser et al. 1983; Sen and Davis 1982; Smith and Davis 1983; Zebib et al. 1985; Smith 1986; Carpenter and Homsy 1990), where thermocapillary flows play a key role in determining crystal quality.

In recent years, the topic of PCM melting with thermocapillary effects in microgravity has been subject of growing research. The problem was first considered in the numerical work of Madruga and Mendoza (2017a, b), an effort that was later extended by the parabolic flight experiments of Ezquerro et al. (2019, 2020). These experiments confirmed, for the first time, the potential of the thermocapillary effect to enhance heat transport during melting in microgravity.

Since these seminal works, a number of numerical studies have looked at this problem from different perspectives. Studies on heat transport of pure PCM (Salgado Sanchez et al. 2020a; Varas et al. 2021; Borshchak Kachalov et al. 2021, 2022) and NePCM (Zhou et al. 2022), pattern selection during phase change (Salgado Sanchez et al. 2021, 2022; Martínez et al. 2021), PCM use for micro-energy harvesting in space applications (Madruga and Mendoza 2022), or wetting properties of melts (Sixue et al. 2021), are a few examples that illustrate the current relevance of this research line.

The majority of these works were obtained using n-octadecane as PCM, due to its moderate $T_M = 28$ °C that makes it attractive for experiments (Ezquerro et al. 2019, 2020) and applications. In this work, we extend these results and analyze the melting in microgravity of other alkanes — n-nonadecane and n-eicosane — and gallium, which represents a completely different type of PCM with large thermal diffusivity. The performance of thermocapillary flows in enhancing heat transport is discussed in terms of the relevant governing parameters and compared in each case. To the best of our knowledge, this work represents the first comparative study of thermocapillary-enhanced melting of different PCMs in microgravity.

Furthermore, we note that the potential of the thermocapillary effect to improve the thermal-control performance of PCMs will be experimentally evaluated by the Marangoni Phase Change Materials (MarPCM) project (Laverón 2021) during a planned series of microgravity experiments on board the International Space Station (ISS). As part of the MarPCM project, the analysis provided here is an important effort to predict and explain the dynamics that are expected to be observed experimentally.

In the same context of microgravity, but without considering thermocapillary effects, other authors have explored the melting process under different configurations of the heat source (Chen et al. 2019; Mahmud and Ahmed 2022).

The manuscript is structured as follows. In "Mathematical Formulation", the mathematical formulation used to model the phase change, and the pertinent details of the numerical simulations are summarized. In "Melting in Microgravity", a basic description of PCM melting in microgravity is provided, including the associated dynamics with and without thermocapillary effects. Results for the different PCMs explored are discussed in "Thermocapillary-enhanced Melting ofdifferent PCMs". Conclusions are offered in "Conclusions".

Mathematical Formulation

The basic problem considered here is the melting of a two-dimensional $L \times H$ rectangular volume of PCM in weightless conditions (i.e., g = 0), driven by imposing constant temperatures T_C and T_H ($> T_C$) on opposite lateral walls. The melting occurs in the presence of an air layer (on top) that supports thermocapillary flows; see Fig. 1. We use an enthalpy-porosity-based formulation of the Navier-Stokes equations to describe the process.

For further details about the mathematical and numerical models, the reader is referred to the works of Salgado Sanchez et al. (2020a, c, 2021).

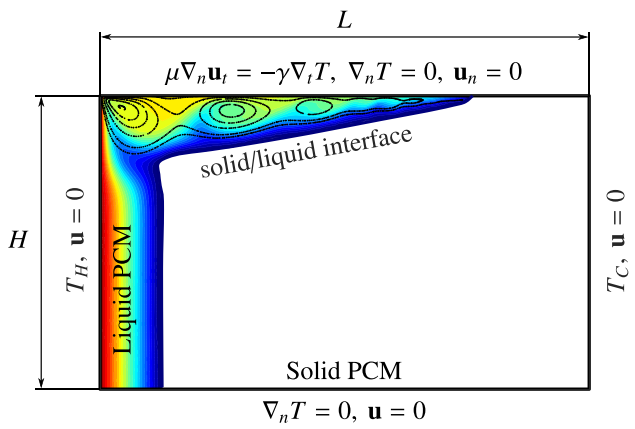

Fig. 1 Sketch of the numerical problem considered. The colormap shows the temperature field within the liquid phase

Governing Equations and Boundary Conditions

The flow in the liquid phase is assumed laminar and incompressible, and is thus described by the Navier-Stokes equations (Landau and Lifshitz 1987),

$$\rho\left(\frac{\partial \mathbf{u}}{\partial t} + (\mathbf{u}\cdot\nabla)\,\mathbf{u}\right) = -\nabla p + \nabla(\mu\,\nabla\mathbf{u}), \tag{1a}$$

$$\nabla\cdot\mathbf{u} = 0, \tag{1b}$$

where $\mathbf{u}$ and p are the velocity and pressure fields, μ is the dynamic viscosity and ρ is the density.

The conservation of energy includes the contributions of sensible and latent heats:

$$\rho c_p\left(\frac{\partial T}{\partial t} + \mathbf{u}\cdot\nabla T\right) = \nabla(k\,\nabla T) - \rho c_L\left(\frac{\partial f}{\partial t} + \mathbf{u}\cdot\nabla f\right), \tag{2}$$

where T is the temperature field, c_p and k denote the specific heat capacity at constant pressure and thermal conductivity, c_L the specific latent heat, and f refers to the local liquid fraction.

During melting, part of the absorbed heat is associated with the fraction of melted PCM through the product $f\rho\,c_L$, with f expressed as a temperature-dependent field modeled using the step function:

$$f(T) = \begin{cases} 0 & \widetilde{T} < -\delta_T/2, \\ \frac{1}{2} + \frac{\widetilde{T}}{\delta_T} + \frac{1}{2\pi}\sin\left(\frac{2\pi\widetilde{T}}{\delta_T}\right) & |\widetilde{T}| \le \delta_T/2, \\ 1 & \widetilde{T} > \delta_T/2, \end{cases} \tag{3}$$

where $\widetilde{T} \equiv T - T_{\mathrm{M}}$. Note that f changes smoothly from 0 to 1 near T_M over a small temperature interval δ_T. This δ_T characterizes the *mushy region* (Egolf and Manz 1994).

We treat the solid and liquid phases as a single phase with properties that depend on T and have appropriate limits for each state. All physical properties of the PCM are expressed using f as follows:

$$\rho = \rho_{\mathrm{S}} + (\rho_{\mathrm{L}} - \rho_{\mathrm{S}})f, \tag{4a}$$

$$\mu = \mu_{\mathrm{S}} + (\mu_{\mathrm{L}} - \mu_{\mathrm{S}})f, \tag{4b}$$

$$c_p = c_{p\mathrm{S}} + (c_{p\mathrm{L}} - c_{p\mathrm{S}})f, \tag{4c}$$

$$k = k_{\mathrm{S}} + (k_{\mathrm{L}} - k_{\mathrm{S}})f, \tag{4d}$$

where the subscripts L and S denote liquid and solid, respectively. Here, we introduce the virtual solid viscosity μ_{S}, a numerical parameter taken several orders of magnitude greater than μ_{L} so that the velocity in the solid phase vanishes (Voller et al. 1987). In accord to previous works, we select a value of $\mu_{\mathrm{S}} = 10^3$ Pa s (Salgado Sanchez et al. 2020a, 2021).

The thermocapillary effect at the PCM-air interface is considered by writing

$$\sigma = \sigma_0 - \gamma\left(T - T_M\right), \tag{5}$$

with the interfacial tension σ depending linearly on T. Here, σ_0 is a reference value at T_M, and $\gamma = |\partial\sigma/\partial T|$ is the thermocapillary coefficient characterizing its variation. In the solid phase ($T \le T_M$), we impose $\gamma = 0$. This dependence of σ on T is the driving force for the thermocapillary flow.

The stress balance at the PCM-air interface includes the contributions of pressure, viscous stress, and surface tension. Experimental (Montanero et al. 2008) and numerical (Shevtsova et al. 2008) research have demonstrated that the interface deformation caused by thermocapillary flows is expected to be on the order of microns. In accord to this, we assume a fixed rectangular domain with a perfectly flat interface, for which the momentum balance simplifies to

$$\mu\nabla_n\mathbf{u}_t = -\gamma\nabla_t T, \tag{6}$$

where the subscripts n and t refer to the normal and tangential components, respectively. The principal error of this simplification is related to the thermal expansion experienced during melting. Even so, the recent work of Salgado Sanchez et al. (2020c) analyzing the melting of n-octadecane in microgravity found good agreement between experiments and simulations that considered the same fixed rectangular domain.

The remaining boundary conditions for T and $\mathbf{u}$ are:

- At the lateral walls:

$$T = T_H,\ T_C; \quad \mathbf{u} = 0. \tag{7}$$

- At the bottom wall:

$$\nabla_n T = 0; \quad \mathbf{u} = 0. \tag{8}$$

- At the PCM-air interface, Eq. (6) is imposed together with

$$\nabla_n T = 0; \quad \mathbf{u}_n = 0. \tag{9}$$

These are indicated in Fig. 1.

We select L, (L^2/α) and $\Delta T = T_H - T_C$, where $\alpha = k_{\mathrm{L}}/(\rho_{\mathrm{L}}c_{p\mathrm{L}})$ is the liquid thermal diffusivity, as characteristics values for length, time and temperature, and the physical properties of the liquid phase for ρ, μ, c_p and k. The dynamics of the system depend on the Marangoni and Stefan numbers

$$\mathrm{Ma} = \frac{\gamma\,L\,\Delta T}{\mu_{\mathrm{L}}\alpha}, \quad \mathrm{Ste} = \frac{c_{p\mathrm{L}}\,\Delta T}{c_L}, \tag{10}$$

the Prandtl number,

$$\mathrm{Pr} = \frac{\mu_\mathrm{L}}{\rho_\mathrm{L}\,\alpha}, \tag{11}$$

the container aspect ratio,

$$\Gamma = \frac{L}{H}, \tag{12}$$

and the ratio of the physical properties in the solid and liquid phases

$$\widetilde{\rho} = \frac{\rho_\mathrm{S}}{\rho_\mathrm{L}}, \quad \widetilde{\mu} = \frac{\mu_\mathrm{S}}{\mu_\mathrm{L}}, \quad \widetilde{k} = \frac{k_\mathrm{S}}{k_\mathrm{L}}, \quad \widetilde{c_p} = \frac{c_{p\mathrm{S}}}{c_{p\mathrm{L}}}. \tag{13}$$

Note that these ratios take fixed values for each choice of PCM.

In this manuscript, melting is analyzed for different PCMs with moderate T_M: n-octadecane, n-nonadecane and n-eicosane — representing three organic materials from the family of alkanes — and gallium. We also consider the (so-called) *test PCM*, which corresponds to a PCM with the properties of n-octadecane and the latent heat of n-nonadecane, to check and adjust δ_T; this is discussed below.

The physical properties and associated dimensionless parameters are detailed in Table 1. Note the selection of n-octadecane due to is relevance to recent experiments (Ezquerro et al. 2019, 2020; Salgado Sanchez et al. 2020c) and simulations (Salgado Sanchez et al. 2020a, 2021, 2022; Borshchak Kachalov et al. 2021, 2022; Varas et al. 2021; Martínez et al. 2021).

Except for gallium, two-dimensional behavior is consistent with the high Pr of these alkanes (Smith and Davis 1983; Peltier and Biringen 1993; Kuhlmann and Albensoeder 2008). We further select $\Gamma = 2.25, 12$ as two representative values of the melting dynamics in short and large containers (Salgado Sanchez et al. 2020a, 2021), using a fixed container length $L = 22.5$ mm. In each case, the remaining dimensionless parameters Ma and Ste are selected by the applied ΔT, which is varied within the interval $\Delta T \in (0, 40)$ K maintaining the cold wall temperature at $T_C = T_M$.

Numerical Simulations

We use COMSOL Multiphysics to solve the formulation described in "Governing Equations and Boundary Conditions" with the finite element method. The initial condition for T is 25 °C, at which the PCMs are in solid state and thus, $\mathbf{u} = 0$. The initial mismatch in T between the interior and boundary values is treated numerically using a Backward Euler scheme for the initial time step. The subsequent time evolution is effected using a Backward Differentiation Formulae scheme with maximum time steps

Table 1 Physical properties (reproduced from Lide (2014)), dimensionless parameters, and mushy region temperature interval δ_T of n-octadecane, n-nonadecane, n-eicosane, gallium and the test PCM

	n-octadecane	n-nonadecane	n-eicosane	gallium	test PCM
Physical properties					
Melting temperature, T_M (°C)	28.0	31.9	37.5	29.8	28.0
Liquid density, ρ_L (kg m^{-3})	780	772	778	6093	780
Solid density, ρ_S (kg m^{-3})	865	780	789	5903	865
Specific latent heat, c_L (kJ kg^{-1})	243.5	170.6	247.3	80.3	170.6
Liquid specific heat capacity, $c_{p\mathrm{L}}$ (J kg^{-1} K^{-1})	2196	2300	2280	397	2196
Solid specific heat capacity, $c_{p\mathrm{S}}$ (J kg^{-1} K^{-1})	1934	1700	2000	373	1934
Liquid conductivity, k_L (W m^{-1} K^{-1})	0.148	0.148	0.150	31.8	0.148
Solid conductivity, k_S (W m^{-1} K^{-1})	0.358	0.260	0.440	40.6	0.358
Dynamic viscosity, μ_L (mPa s)	3.54	3.49	3.20	1.10	3.54
Thermocapillary coefficient, γ (N m^{-1} K^{-1} $\times 10^{-5}$)	8.44	10	9.8	6.8	8.44
Thermal diffusivity, α (m^2 s^{-1} $\times 10^{-8}$)	8.6	8.3	9.6	1310	8.6
Dimensionless parameters					
Prandtl number, Pr	52.7	54.5	42.8	0.01	52.7
Density ratio, $\widetilde{\rho}$	1.11	1.01	1.01	0.97	1.11
Conductivity ratio, $\widetilde{k}$	2.42	1.76	2.93	1.28	2.42
Heat capacity ratio, $\widetilde{c_p}$	0.88	0.74	0.87	0.94	0.88
Ma/Ste, $\mathcal{K} \times 10^{-5}$	6.88	5.74	7.79	0.12	4.82
Mushy region interval, δ_T (K)	1.00[a]	0.67	0.98	1.82	0.70

[a]Reproduced from Salgado Sanchez et al. (2020c)

of $\Delta t \in [0.0005, 0.01]$ s depending on ΔT, and stabilized with streamline (Harari and Hughes 1992) and crosswind (Codina 1993) schemes.

The mesh selection criteria follows previous works with a maximum element size of $\mathcal{S} = L/67.5$ if $\Gamma = 2.25$, or $(2/3)\mathcal{S}$ if $\Gamma = 12$; further details of convergence tests can be found in Salgado Sanchez et al. (2020a, 2021). We apply a local mesh refinement near the thermocapillary interface to better capture the enhanced melting evolution associated with the thermocapillary flow. The criterium used to select δ_T is discussed hereafter.

Mushy Region Temperature Interval

The use of an enthalpy-porosity formulation introduces the numerical parameter δ_T. For n-octadecane, different δ_T values were reported in the literature ranging between 1 to 4 K, depending on the purity of the sample and the experimental technique (Ho and Gaoe 2009; Velez et al. 2015). Following the work of Salgado Sanchez et al. (2020a, 2021), melting dynamics for n-octadecane are solved using $\delta_T^* = 1$ K. The corresponding δ_T values for the other PCMs are adjusted consistently to this selection as described below.

We consider the additional dimensionless parameter

$$\widetilde{\delta} = \frac{\delta_T}{\Delta T}, \tag{14}$$

which needs to be preserved between PCMs to permit the comparison.

As a reference, melting under purely diffusive transport ($\gamma = 0$) of the test PCM is considered first. Note that the associated melting time τ_{ref}, when all the PCM volume becomes liquid, should be equal to that of n-octadecane if Ste is preserved. This condition reads

$$\text{Ste}^* = \left(\frac{c_{p\text{L}}\Delta T}{c_L}\right)^* = \frac{c_{p\text{L}}\Delta T}{c_L} = \text{Ste}, \tag{15}$$

where the superscript '$_*$' refers to (the values of) n-octadecane. Therefore, the applied temperature difference ΔT that provides an equal melting time for the test PCM is

$$\Delta T = \Delta T^* \left(\frac{c_L}{c_L^*}\right)\left(\frac{c_{p\text{L}}^*}{c_{p\text{L}}}\right), \tag{16}$$

and thus, the associated value of δ_T that preserves $\widetilde{\delta}$ is

$$\delta_T = \delta_T^*\left(\frac{\Delta T}{\Delta T^*}\right) = \delta_T^*\left(\frac{c_L}{c_L^*}\right)\left(\frac{c_{p\text{L}}^*}{c_{p\text{L}}}\right); \tag{17}$$

recall that $\delta_T^* = 1$ K. Anticipate that the melting time in reference simulations (i.e., without thermocapillary effects) are shown below in Fig. 3 of "Melting in Microgravity" for n-octadecane (black) and the test PCM (green). Note that both curves perfectly overlap.

Following the same argument, one can obtain consistent δ_T values for each PCM; these are summarized in Table 1.

Melting in Microgravity

We first describe the melting dynamics in microgravity and compare the (so-called) reference process under purely diffusive conditions (conduction) with that driven by thermocapillary effects. In Fig. 2, four snapshots at selected times (labeled) illustrate the associated phase change evolutions for n-octadecane and $\Gamma = 2.25$. Results are shown for an applied $\Delta T = 30$ K, which corresponds to Ste = 0.271 and Ma = 186224 in the thermocapillary case.

The reference melting is represented by the progression of the solid/liquid (S/L) front (black line), i.e., the $T = T_M$ isotherm. As can be seen in the figure, the front advances parallel to the hot wall, reflecting one-dimensional behavior. In addition, note that the melting rate decreases as the S/L front separates from the hot wall, as it does the effective thermal gradient within the liquid phase. For further details, the reader is referred to the work of Salgado Sanchez et al. (2020a).

The thermocapillary-enhanced melting, on the other hand, is illustrated by the temperature distribution in the liquid phase (colormap). As described in Salgado Sanchez et al. (2020a, 2021), the very beginning of the process is dominated by conduction, with a characteristic advance of

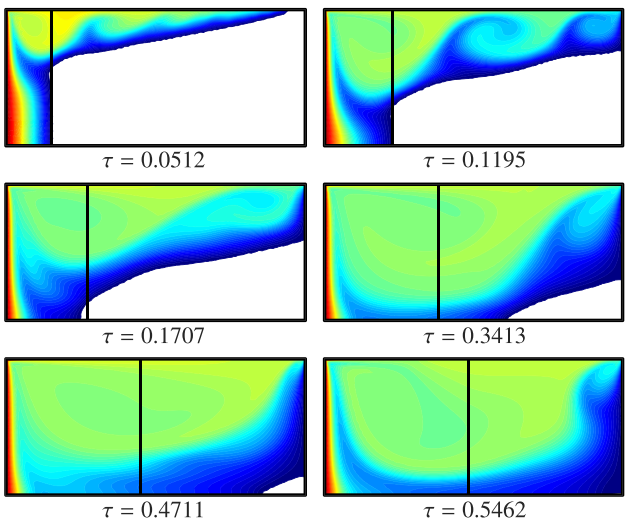

Fig. 2 Snapshots showing the melting evolution for n-octadecane, $\Gamma = 2.25$ and Ste = 0.271 ($\Delta T = 30$ K); this corresponds to Ma = 186224 in the thermocapillary case. The colormap shows the temperature field within the liquid phase and the black vertical line indicates the position of the S/L front in the thermocapillary and reference cases, respectively. The figure is adapted from Salgado Sanchez et al. (2020a)

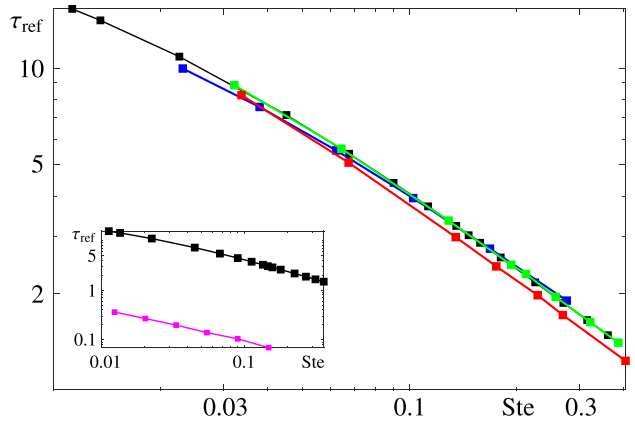

Fig. 3 Reference melting times τ_{ref} as a function of Ste for n-octadecane (black), n-nonadecane (red), n-eicosane (blue), the test PCM (green), and gallium (pink), illustrated in the inset

the S/L front parallel to the hot lateral wall, analogous to that of the reference case. Near the PCM-air interface, the thermocapillary effect acts drawing hot liquid from the hot wall toward the S/L front, which remains at T_M, fact that accelerates melting locally, as evidenced at $\tau = 0.0512$. Note that there are two well-differentiated regions: one upper region affected by the thermocapillary flow, and one lower region that reflects the behavior of a phase change driven by thermal diffusion.

In the thermocapillary region, the accelerated melting persists until the S/L front reaches the cold wall, when it cannot proceed further horizontally; see the snapshot at $\tau = 0.1195$. From this point onward, the melting evolution near the cold wall is characterized by a downward progression of the front. As discussed in Salgado Sanchez et al. (2021) for $\Gamma = 2.25$, the flow becomes oscillatory in the form of an oscillatory standing wave (OSW) at a critical Marangoni number $\mathrm{Ma}_{cr} \simeq 68852$, corresponding with a critical Ste and applied temperature difference of $\mathrm{Ste}_{cr} \simeq 0.1$ and $\Delta T_{cr} \simeq 11.1$ K. For this applied Ma = 186224 ($> \mathrm{Ma}_{cr}$), therefore, OSWs are observed in the liquid phase during the melting process. The reader is referred to Salgado Sanchez et al. (2021) for further details.

The melting with thermocapillary effects is completed by $\tau_{\mathrm{Ma}} \simeq 0.5462$, time at which the S/L front in the reference simulation has not yet reached the central plane of the PCM volume; melting rate is thus enhanced by a factor of, at least, 2. Below, we quantify the contribution of the thermocapillary effect to the overall heat transfer rate by comparing the dimensionless melting times in both scenarios, τ_{Ma} and τ_{ref}

$$\left(\tau_{\mathrm{Ma}},\ \tau_{\mathrm{ref}}\right) = \left(\frac{\alpha}{L^2}\right)\left(t_{\mathrm{Ma}},\ t_{\mathrm{ref}}\right), \tag{18}$$

where t_{Ma} and t_{ref} are the times at which the melting is completed (i.e., all the solid PCM is melted); the reader is referred again to Salgado Sanchez et al. (2020a, 2021) for a more detailed analysis.

For the other explored PCMs, the reference melting times τ_{ref} are shown in Fig. 3 as a function of Ste. Note that, as anticipated above, the curves for n-octadecane (black) and the test PCM (green) overlap. Results for n-nonadecane (red) and n-eicosane (blue) are also quite similar, which demonstrates that small changes in the thermophysical properties do not substantially affect the phase change process. Reference times for gallium, in contrast, are substantially smaller than those obtained for alkanes. It is the large thermal diffusivity of gallium, which surpasses by two orders of magnitude that of the alkanes, the property that reflects a more effective conductive heat transfer and thus, melting times that are about two orders of magnitude smaller.

Now, we extend these results and analyze the melting of different PCMs with thermocapillary effects.

Thermocapillary-enhanced Melting of Different PCMs

The Test PCM

To isolate the influence of Ste, the test PCM is analyzed first, and compared against n-octadecane; the associated results are adapted from Salgado Sanchez et al. (2020a). Note that, for a fixed ΔT, all dimensionless parameters except Ste are held constant between both PCMs.

The overall melting evolution is analogous to that described in "Melting in Microgravity" for n-octadecane. We characterize it by looking at the melting time τ_{Ma} for different applied Ma; these are shown in Fig. 4 for two representative aspect ratios $\Gamma = 2.25,\ 12$, including the corresponding results for n-octadecane for comparison.

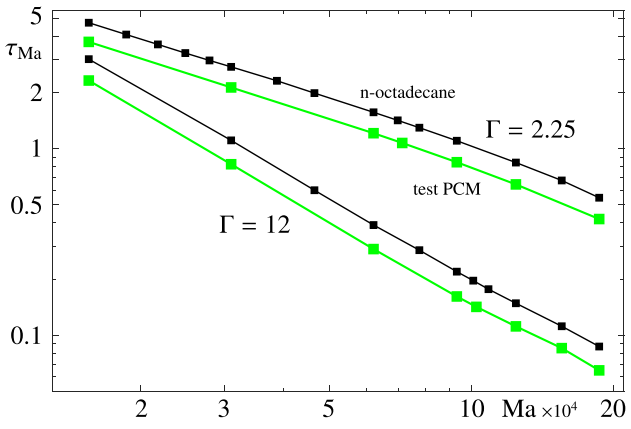

Fig. 4 Melting times τ_{Ma} as a function of Ma for n-octadecane (black) and the test PCM (green) at two selected aspect ratios $\Gamma = 2.25,\ 12$

Over the explored range of Ma, a nearly constant reduction of 25–29% in τ_{Ma} is evident with respect to n-octadecane, consistent with the lower latent heat of the test PCM. It can be further noted a larger dependence (in absolute value) of τ_{Ma} on Ma for $\Gamma = 12$. This clearly reflects the increased importance of thermocapillary effects in large containers during melting (Salgado Sanchez et al. 2020a).

These results can be also discussed in terms of the relevant dimensionless parameters, Ma and Ste. For a fixed applied ΔT, Ma and Ste obey the following linear relationship

$$\mathrm{Ma} = \frac{c_L \gamma L}{c_{p\mathrm{L}} \mu_{\mathrm{L}} \alpha} \mathrm{Ste} = \mathcal{K}\,\mathrm{Ste}, \tag{19}$$

where $\mathcal{K} = 6.88 \times 10^5$, 4.82×10^5 for n-octadecane and the test PCM, respectively. For a fixed applied Ma, the test PCM is subjected to a Ste that is 1.43 times larger than that of n-octadecane. This quantifies a diminishing (increasing) importance of the latent heat (sensible heat) during melting. From a physical point of view, a reduced latent heat reflects a smaller storage capacity of the PCM and is thus associated with faster melting.

This idea can be extrapolated to the different alkanes considered, allowing to anticipate the overall melting behavior by simply comparing Ma and Ste with that of n-octadecane; recall the weak influence of the other dimensionless parameters (i.e., ratio of thermophysical properties between the solid and liquid phases) discussed above and the similar Pr. For n-nonadecane and n-eicosane, the relationship between Ma and Ste is characterized by $\mathcal{K} = 5.74 \times 10^5$, 7.79×10^5, respectively. In Fig. 5, the curves Ma vs. Ste are illustrated in each case, where markers denote particular values used for simulations.

N-nonadecane

As detailed in Table 1, the physical properties of n-nonadecane are quite similar to those of n-octadecane, except for its latent heat, which is approximately a 30% smaller. Following the previous discussion, melting times for n-nonadecane are thus expected to be smaller.

In this case, Ste values for a fixed applied Ma are larger by a factor of 1.20 with respect to n-octadecane, and slightly smaller than those of the test PCM. This helps explain the results shown in Fig. 6, with τ_{Ma} that are roughly 20% smaller than for n-octadecane, and 10% larger than those obtained for the test PCM. Again, the comparison between panels (a, b) of Fig. 6 reflects an increased influence of thermocapillary effects in large containers: while τ_{Ma} decreases one order of magnitude in panel (a), a reduction by two orders of magnitude is observed in panel (b) within the same interval of Ma.

To characterize the overall effectiveness of the thermocapillary effect in enhancing heat transport, we follow previous works (Salgado Sanchez et al. 2020a; Borshchak Kachalov et al. 2021; Varas et al. 2021) and define the enhancement factor $\mathcal{G}$ as

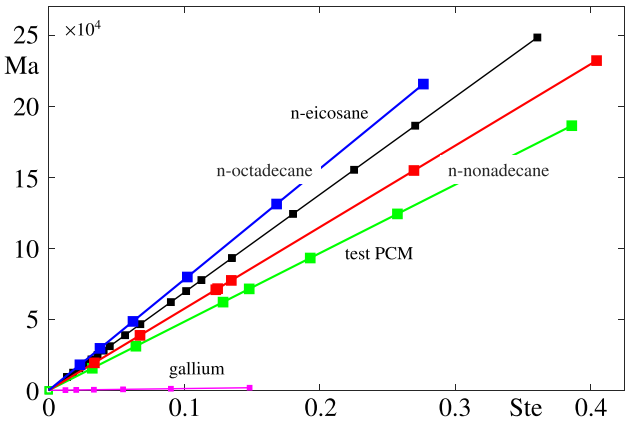

Fig. 5 Comparison between Ste and Ma for each PCM

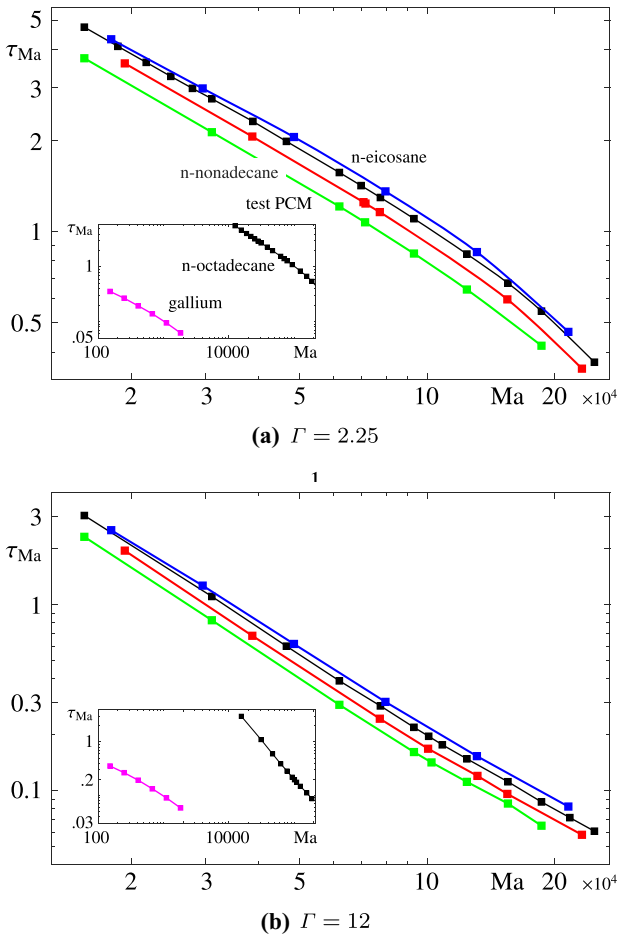

Fig. 6 Melting times τ_{Ma} as a function of Ma for n-octadecane (black), n-nonadecane (red), n-eicosane (blue), the test PCM (green), and gallium (pink), and two selected aspect ratios **(a)** $\Gamma = 2.25$, **(b)** $\Gamma = 12$

$$\mathcal{G} = \frac{\tau_{\text{ref}}}{\tau_{\text{Ma}}}, \tag{20}$$

which simply compares times for complete melting between the reference and thermocapillary scenarios. In Fig. 7, the factor $\mathcal{G}$ is illustrated as a function of Ma for n-octadecane (black), n-nonadecane (red), n-eicosane (blue) and gallium (pink), and the selected aspect ratios (a) $\Gamma = 2.25$, (b) $\Gamma = 12$. Since the test PCM was only considered to adjust the numerical model, we do not include here its enhancement factor.

Compared to n-octadecane, the overall enhancement achieved for n-nonadecane is reduced. Again, one can explain this in terms of dimensionless parameters. Provided an equal influence of the latent heat during melting, as measured by a constant Ste, the applied Ma for n-octadecane is 1.43 times larger than for n-nonadecane. This quantifies an increased importance of the thermocapillary effect that is reflected in larger $\mathcal{G}$.

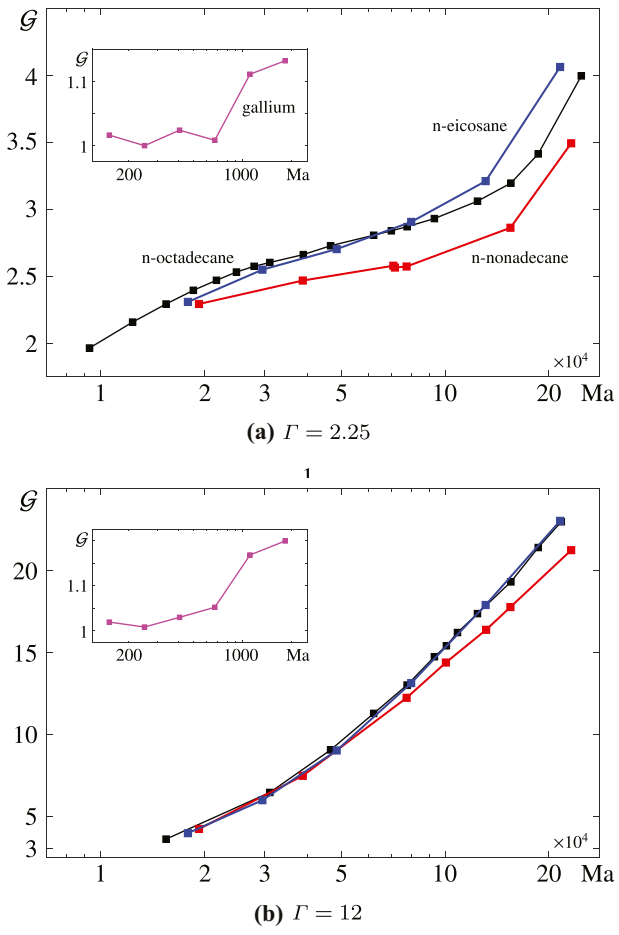

Fig. 7 Enhancement factor $\mathcal{G}$ as a function of Ma for n-octadecane (black), n-nonadecane (red), n-eicosane (blue) and gallium (pink), and two selected aspect ratios **(a)** $\Gamma = 2.25$, **(b)** $\Gamma = 12$

In accord with previous works (Salgado Sanchez et al. 2020a; Varas et al. 2021), note the achieved values of $\mathcal{G}$ in large containers can be up to 20 for large applied Ma, while they are reduced to 2-4 in shorter ones.

N-eicosane

Similarly, now we analyze the results for n-eicosane. Like other alkanes, it displays good compatibility properties with structural materials and low tendency to corrosion. Its physical properties are also similar to those of n-octadecane, except for its value of T_M, which is approximately 10 K larger; recall that these are summarized in Table 1.

According to Fig. 5, n-eicosane presents the lowest Ste values for any Ma. Therefore, it is expected to be more affected by the absorption of latent heat during melting, and exhibit the longest melting times τ_{Ma}, as shown in Fig. 6.

In line with this, n-eicosane is expected to present the largest values of $\mathcal{G}$, as shown in Fig. 7 for $\text{Ma} > 5 \times 10^4$, supported by a higher Ma at fixed Ste, quantifying the increased relevance of thermocapillary effects. For $\text{Ma} < 5 \times 10^4$, where thermocapillary effects are less relevant, the values of $\mathcal{G}$ are slightly reduced compared to n-octadecane; this can be explained in terms of α, which is larger for n-eicosane.

In short containers, the values of $\mathcal{G}$ for n-eicosane are lower (but still similar) than those of n-octadecane, suggesting an increased importance of the latent heat in the melting process.

Gallium

Gallium is a metallic PCM and one of the few materials that expand during solidification. It displays large chemical and physical stability, but high tendency to corrosion when put in contact with aluminum and most metals, except titanium. It also displays good compatibility with ceramics.

We include the analysis of this PCM to explore a completely different type of material, with properties that differ from the alkane family. As detailed in Table 1, one of the largest differences is in its thermal diffusivity, which is up to two orders of magnitude higher; this large value is associated with a small Pr. As a side note for microgravity applications, it presents a major disadvantage related to its high density and associated mass.

As shown in Figs. 6 and 7, results are substantially different compared to previous cases. Again, these can be explained looking at the relationship between Ma and Ste that is now characterized by a value of $\mathcal{K} = 1.23 \times 10^4$, one order of magnitude smaller than for alkanes.

Following previous arguments, gallium displays Ste numbers that are one order of magnitude larger at a fixed applied Ma, which are associated with reduced τ_{Ma}. It is the high thermal diffusivity of gallium that makes the whole

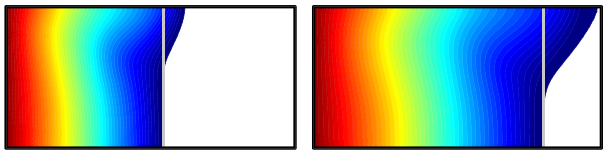

Fig. 8 Snapshots (times indicated) showing the evolution of the phase change for gallium at Ma = 1212 (Ste = 0.099) for $\Gamma = 2.25$. The colormap shows the temperature field within the liquid phase and the black grey line indicates the position of the S/L front in the thermocapillary and reference cases, respectively

process being dominated by conduction and reduces the relative importance of the thermocapillary effect. For realistic values of ΔT, the applied Ma is significantly lower than for alkanes, barely reaching 1800.

Given that the thermocapillary effect has a low impact on the melting, the reference and thermocapillary cases are very similar. Overall, the effect of thermocapillary flow improves the melting rate by a factor as large as a 20%, which is less significant than the enhancement obtained for alkanes. This reduction can be seen in Fig. 7, where gallium exhibits values of $\mathcal{G}$ close to unity, with a maximum of 1.2 for $\Gamma = 12$, reinforcing the idea that the melting process is dominated by thermal diffusion rather than the convective transport supported by the thermocapillary effect.

To illustrate this, Fig. 8 includes two snapshots of the reference and thermocapillary-driven melting evolutions for gallium, $\Gamma = 2.25$ and Ste = 0.099. As in Fig. 2, the reference melting is represented by the progression of the $T = T_M$ isotherm, marked with a gray line, while the thermocapillary-driven melting is illustrated by the temperature distribution in the liquid phase (colormap). Compared to the results described in "Melting in Microgravity", the melting processes here are arguably similar, fact that justifies the limited values of $\mathcal{G}$ associated to this PCM.

Conclusions

This paper presented a numerical study of PCM melting with thermocapillary effects in microgravity. The phase change was described using an enthalpy-porosity formulation of the Navier-Stokes equations, which models the coexisting solid and liquid states as a single phase with physical properties that depend on temperature and change sharply across the solid/liquid front.

Melting was analyzed for different PCMs with moderate melting temperature T_M, due to their potential for thermal control in space applications. We considered three different alkanes — n-octadecane, n-nonadecane and n-eicosane — and gallium. Results were discussed in terms of the Stefan (Ste) and Marangoni (Ma) numbers, which quantify the importance of latent heat and the thermocapillary effect during melting, respectively, and the aspect ratio Γ, characterizing the geometry of the container.

Similar results were obtained for alkanes, with enhancement factors $\mathcal{G}$ that depend strongly on Γ. In short containers, represented by $\Gamma = 2.25$, the thermocapillary effect improved the melting rate by a factor up to 4 depending on Ma. The largest improvements of the melting rate were obtained for n-eicosane, showing stronger thermocapillary enhancement for smaller Ste at a fixed Ma. In large containers, which were represented by $\Gamma = 12$, the values of $\mathcal{G}$ ranged between 5 and 20 depending on Ma for all alkanes. Again, this improvement was slightly better for n-octadecane and n-eicosane.

For gallium, results differed substantially due to its large thermal diffusivity. The melting process for this PCM was shown to be dominated by conduction instead of the convective transport supported by thermocapillary flows, reducing the associated enhancement. Overall, the reference and thermocapillary cases were quite similar for gallium, and the thermocapillary effect only improved the heat transfer rate by a factor $\mathcal{G}$ of as much as a 20% over the explored range of parameters.

Finally, we recall that the present work represents a significant part of the MarPCM project that will analyze the effectiveness of thermocapillary flows to increase the heat transfer rate of PCMs. A series of microgravity experiments onboard the ISS will evaluate the heat transport enhancement and any possible issues related to the operation of a thermocapillary-enhanced PCM in microgravity, including the potentially difficult task of maintaining a stable free surface over repeated melting and solidification cycles.

Acknowledgements This work was supported by the Ministerio de Ciencia e Innovación under Project No. PID2020-115086GB-C31, and by the Spanish User Support and Operations Centre (E-USOC), Center for Computational Simulation (CCS).

Author Contributions NG and JJ conducted the analysis. PS, UM, and JME prepared the figures, the original and the revised versions of the manuscript. PS and JME supervised the investigation. All authors reviewed the manuscript.

Funding Open Access funding provided thanks to the CRUE-CSIC agreement with Springer Nature. Ministerio de Ciencia e Innovación, Project No. PID2020-115086GB-C31.

Availability of Data and Material All data is available within the manuscript.

Declarations

Ethics Approval Not applicable.

Consent to Participate Not applicable.

Consent for Publication Not applicable.

Conflicts of Interest The authors declare no competing interests.

References

Agyenim, F., Eames, P., Smyth, M.: A comparison of heat transfer enhancement in a medium temperature thermal energy storage heat exchanger using fins. Sol. Energy **83**, 1509–1520 (2009)

Atal, A., Wang, Y., Harsha, M., Sengupta, S.: Effect of porosity of conducting matrix on a phase change energy storage device. Journal of Heat and Mass Transfer **93**, 9–16 (2016)

Biwole, P.H., Eclache, P., Kuznik, F.: Phase change materials to improve solar panel's performace. Energy and Buildings **62**, 59–67 (2013)

Borshchak Kachalov, A., Salgado Sanchez, P., Porter, J., Ezquerro, J.M.: The combined effect of natural and thermocapillary convection on the melting of phase change materials in rectangular containers. Int. J. Heat Mass Transf. **168**, 120864 (2021)

Borshchak Kachalov, A., Salgado Sánchez, P., Martínez, U., Fernández, J., Ezquerro, J.M.: Optimization of thermocapillary-driven melting in trapezoidal and triangular geometry in microgravity. Int. J. Heat Mass Transf. **185**, 122427 (2022)

Cabeza, L., Mehling, H., Hiebler, S., Ziegler, F.: Heat transfer enhancement in water when used as PCM in thermal energy storage. Appl. Therm. Eng. **22**, 1141–1151 (2002)

Carpenter, B.M., Homsy, G.M.: High Marangoni number convection in a square cavity: Part II. Phys. Fluids **2**, 137–149 (1990)

Chaiyat, N., Kiatsiriroat, T.: Energy reduction of building air-conditioner with phase change material in thailand. Case Studies in Thermal Engineering **4**, 175–186 (2014)

Chen, X., Hao, G., Yao, F., Zhang, C.: Numerical study on melting phase change under microgravity. Microgravity Sci. Technol. **31**, 793–803 (2019)

Codina, R.: A discontinuity-capturing crosswind-dissipation for the finite element solution of the convection-diffusion equation. Comput. Methods Appl. Mech. Eng. **110**, 325–342 (1993)

Creel, R.: Apollo rover lessons learned: applying thermal control experiences on Apollo Lunar Rover project to rovers for future space exploration. (2007)

Dhaidan, N.S., Khodadadi, J.M.: Melting and convection of phase change materials in different shape containers: A review. Renew. Sustain. Energy Rev. **43**, 449–477 (2015)

Dhaidan, N.S., Khodadadi, J.M., Al-Hattab, T.A., Al-Mashat, S.M.: Experimental and numerical investigation of melting of NePCM inside an annular container under a constant heat flux including the effect of eccentricity. Int. J. Heat Mass Transf. **67**, 455–468 (2013)

Egolf, P.W., Manz, H.: Theory and modeling of phase change materials with and without mushy regions. Int. J. Heat Mass Transf. **37**, 2917–2924 (1994)

Ettouney, H.M., Alatiqi, I., Al-Sahali, M., Al-Ali, S.A.: Heat transfer enhancement by metal screens and metal spheres in phase change energy storage systems. Renewable Energy **29**, 841–860 (2004)

Ezquerro, J.M., Bello, A., Salgado Sanchez, P., Laveron-Simavilla, A., Lapuerta, V.: The Thermocapillary Effects in Phase Change Materials in Microgravity experiment: design, preparation and execution of a parabolic flight experiment. Acta Astronaut. **162**, 185–196 (2019)

Ezquerro, J.M., Salgado Sanchez, P., Bello, A., Rodriguez, J., Lapuerta, V., Laveron-Simavilla, A.: Experimental evidence of thermocapillarity in Phase Change Materials in microgravity: measuring the effect of marangoni convection in solid/liquid phase transitions. Int. Commun. Heat Mass Transfer **113**, 104529 (2020)

Fernandes, D., Pitie, F., Caceres, G., Baeyens, J.: Thermal energy storage: "how previous findings determine current research priorities." Energy **39**, 246–257 (2012)

Harari, I., Hughes, T.: What are C and h?: Inequalities for the analysis and design of finite element methods. Comput. Methods Appl. Mech. Eng. **97**, 157–192 (1992)

Higuera, F.J.: Liquid-fuel thermocapillary flow induced by a spreading flame. J. Fluid Mech. **473**, 349–377 (2002)

Ho, C.J., Gaoe, J.Y.: Preparation and thermophysical properties of nanoparticle-in-paraffin emulsion as phase change material. Int. Commun. Heat Mass Transfer **36**, 467–470 (2009)

Ho, C.J., Jou, B.T., Lai, C.M., Huang, C.Y.: Performance assessment of a BIPV integrated with a layer of water-saturated MEPCM. Energy and Buildings **67**, 322–333 (2013)

Hosseinizadeh, S.F., Darzi, A.A.R., Tan, F.L.: Numerical investigations of unconstrained melting of nano-enhanced phase change material (NEPCM) inside a spherical container. Int. J. Therm. Sci. **51**, 77–83 (2012)

Kim, T.Y., Hyun, B.S., Lee, J.J., Rhee, J.: Numerical study of the spacecraft thermal control hardware combining solid-liquid phase change material and a heat pipe. Aerospace Sciences and Technology **27**, 10–16 (2013)

Kuhlmann, H.C., Albensoeder, S.: Three-dimensional flow instabilities in a thermocapillary-driven cavity. Phys. Rev. E **77**, 036303 (2008)

Landau, L.D., Lifshitz, E.M.: Fluid mechanics. Pergamon Books Ltd. (1987)

Lane, G.A.: Solar Heat Storage: Latent Heat Material - Volume 1: Background and Scientific Principles. (1983)

Laverón, A.: Experiment Scientific Requirement (ESR) document: Effect of Marangoni Convection on Heat Transfer in Phase Change Materials. Ref: ESA-HRE-ESR-Marangoni in PCM, Iss. 1, Rev 2. (2021)

Lee, K.O., Medina, M.A.: Using phase change materials for residential air conditioning peak demand reduction and energy conservation in coastal and transitional climates in the state of California. Energy and Buildings **116**, 69–77 (2016)

Lide, D.R.: Handbook of Chemistry and Physics. (2014)

Madruga, S., Mendoza, C.: Enhancement of heat transfer rate on phase change materials with thermocapillary flows. Eur. Phys. J. Spec. Top. **226**, 1169–1176 (2017a)

Madruga, S., Mendoza, C.: Heat transfer performance and melting dynamic of a phase change material subjected to thermocapillary effects. Int. J. Heat Mass Transf. **109**, 501–510 (2017b)

Madruga, S., Mendoza, C.: Introducing a new concept for enhanced micro-energy harvesting of thermal fluctuations through the marangoni effect. Appl. Energy **306**, 117966 (2022)

Mahmud, H., Ahmed, D.H.: Numerical investigations on melting of phase change material (pcm) with different arrangements of heat source-sink pairs under microgravity. Microgravity Sci. Technol. **34**, 20 (2022)

Martínez, N., Salgado Sanchez, P., Porter, J., Ezquerro, J.M.: Effect of surface heat exchange on phase change materials melting with thermocapillary flow in microgravity. Phys. Fluids **33**, 083611 (2021)

Mishra, D.K., Bhowmik, S., Pandey, K.M.: Analysis of heat transfer rate for different annulus shape properties-enhanced beeswax-based phase change material for thermal energy storage. Math. Probl. Eng. **2022**, 21 (2022)

Montanero, J.M., Ferrero, C., Shevtsova, V.M.: Experimental study of the free surface deformation due to thermal convection in liquid bridges. Experiments and Fluids **45**, 1087–1101 (2008)

Peltier, L.J., Biringen, S.: Time-dependent thermocapillary convection in a rectangular cavity: numerical results for a moderate Prandtl number fluid. J. Fluid Mech. **257**, 339–357 (1993)

Preisser, F., Schwabe, D., Scharmann, A.: Steady and oscillatory thermocapillary convection in liquid columns with free cylindrical surface. J. Fluid Mech. **126**, 545–567 (1983)

Salgado Sanchez, P., Ezquerro, J.M., Fernandez, J., Rodriguez, J.: Thermocapillary effects during the melting of phase change materials in microgravity: heat transport enhancement. Int. J. Heat Mass Transf. **163**, 120478 (2020a)

Salgado Sanchez, P., Ezquerro, J.M., Porter, J., Fernandez, J., Rodriguez, J., Tinao, I., Lapuerta, V., Laveron-Simavilla, A., Ruiz, X., Gavalda, F., Mounir Bou-Ali, M.M., Ortiz, J.: The effect of thermocapillary convection on PCM melting in microgravity: results and expectations. Proceeding of the 72th International Astronautical Conference (IAC) (2020b)

Salgado Sanchez, P., Ezquerro, J.M., Porter, J., Fernandez, J., Tinao, I.: Effect of thermocapillary convection on the melting of Phase Change Materials in microgravity: experiments and simulations. Int. J. Heat Mass Transf.**154**, 119717 (2020c)

Salgado Sanchez, P., Ezquerro, J.M., Fernandez, J., Rodriguez, J.: Thermocapillary effects during the melting of Phase Change Materials in microgravity: steady and oscillatory flow regimes. J. Fluid Mech. **908**, A20 (2021)

Salgado Sanchez, P., Porter, J., Ezquerro, J.M., Tinao, I., Laveron-Simavilla, A.: Pattern selection for thermocapillary flow in rectangular containers in microgravity. Phys. Rev. Fluids **7**, 053502 (2022)

Samanta, S.K.: Interdisciplinary issues in materials processing and manufacturing. American Society of Mechanical Engineers, New York (1987)

Schwabe, D., Scharmann, A.: Some evidence for the existence and magnitude of a critical marangoni number of the onset of oscillatory flow in crystal growth melts. J. Cryst. Growth **46**, 125–131 (1979)

Sen, A.K., Davis, S.H.: Steady thermocapillary flows in two-dimensional slots. J. Fluid Mech. **121**, 163–186 (1982)

Shevtsova, V., Mialdun, A., Ferrera, C., Ermakov, M., Cabezas, M.G., Montanero, J.: Subcritical and oscillatory dynamic surface deformations in non-cylindrical liquid bridges. Fluid Dyn. Mater. Process. **4**, 43–54 (2008)

Shuja, S.Z., Yilbas, B.S., Momin, O.: Laser repetitive pulse heating and melt pool formation at the surface. J. Mech. Sci. Technol. **25**, 479–487 (2011)

Sirignano, W.A., Glassman, I.: Flame spreading above liquid fuels: Surface tension driven flows. Combust. Sci. Technol. **1**, 307 (1970)

Sixue, W., Shi, H., Xiaoqing, W., Jianqiang, L., Qiang, Y., Xiaoyu, L., Yuehai, W., Keqing, N.: Research on melt wettability measurements under microgravity. Microgravity Sci. Technol. **33**, 17 (2021)

Smith, M.K.: Instability mechanisms in dynamic thermocapillary liquid layers. Phys. Fluids **29**, 3182 (1986)

Smith, M.K., Davis, S.H.: Instabilities of dynamic thermocapillary liquid layers. Part 1. Convective instabilities. J. Fluid Mech. **132**, 119–144 (1983)

Varas, R., Salgado Sanchez, P., Porter, J., Ezquerro, J.M., Lapuerta, V.: Thermocapillary effects during the melting in microgravity of phase change materials with a liquid bridge geometry. Int. J. Heat Mass Transf. **178**, 121586 (2021)

Velez, C., Khayet, M., Ortiz, J.M.: Temperature-dependent thermal properties of solid/liquid phase change even-numbered n-alkanes: n-Hexadecane, n-octadecane and n-eicosane. Appl. Energy **143**, 383–394 (2015)

Voller, V.R., Cross, M., Markatos, N.C.: An enthalpy method for convection/diffusion phase change. Int. J. Numer. Meth. Eng. **24**, 271–284 (1987)

Zebib, A., Homsy, G.M., Meiburg, E.: High Marangoni number convection in a square cavity. Phys. Fluids **28**, 3467–3476 (1985)

Zhou, X., Duan, W., Chi, F., Jiang, Y.: Numerical investigation of Nano-PCM melting enhanced by thermocapillary convection under microgravity conditions. Microgravity Sci. Technol. 34–41 (2022)